




Size effects of precursor droplets on lithium-based nanomaterial synthesis using flame spray pyrolysis

Ruitian He, Jingqi Gao, Kai H. Luo^{*} 

Department of Mechanical Engineering, University College London, Torrington Place, London, WC1E 7JE, UK

ARTICLE INFO

Keywords:

Nanoparticles synthesis
Lithium precursors
Flame spray pyrolysis
Size effect
Reactive molecular dynamics

ABSTRACT

The initial size of precursor droplets is one of the few control parameters in flame spray synthesis of energy nanomaterials with profound but poorly understood effects. This study unravels the influence of the initial lithium precursor droplet size on the reaction kinetics and formation mechanism of lithium nanoparticles. The reactive molecular dynamics simulations are performed, followed by comprehensive analyses of the droplet's morphology and kinetic and potential energy evolutions, bond kinetics, gas decomposition and reaction pathways of synthesized lithium nanoparticles. The droplet volume keeps rising over time, accompanied by the gradual formation of a hollow structure, which can be interpreted by the predominant role of gas decomposition in shaping the droplet's morphology. As the droplet size increases, however, the explosion behaviour becomes less intense. Besides, more lithium atoms agglomerate to form larger lithium nanoparticles, as evidenced by the increased lithium bond number and reduced atomic mean squared displacements. The reaction pathways also suggest that randomly dispersed small lithium nanoparticles ultimately aggregate to form larger lithium clusters. When the ambient temperature is decreased, the initial droplet size has a more pronounced effect on the size of synthesized lithium clusters, primarily attributed to the reduced reactivity and increased stability of lithium nanoparticles.

1. Introduction

Since the first commercial lithium ion batteries (LIBs) were produced by Sony in 1991 [1], tremendous efforts have been devoted to enhancing their performance, accelerated by the global trend towards decarbonization [2]. The electrochemical performance of cathodes depends on numerous factors, such as the cathode nanoparticle size, morphology, and porosity [3,4]. In particular, the nanoparticle size is regarded as one of the major factors affecting the capacity and rechargeability of cathodes [5]. This is because it can significantly influence the kinetic properties of cathode nanomaterials, through offering short diffusion paths for lithium ions in the electrodes [6,7]. Meanwhile, it can result in a higher reactivity by providing a greater specific surface area, and a better cycle stability due to peculiarly stable mechanical structure [6,8,9]. However, conventional synthetic routes place some limitations in producing fine-sized particles in cathode materials [2,10]. For example, the solid-state reaction synthetic method, though effective and easily scaled to industrial level [2], requires additional mechanical ball-milling post-treatment for particle size reduction. In addition, it suffers from

long sintering time [11], low homogeneity and uncontrolled morphology in final products [2], making it inappropriate for the synthesis of fine-structured materials [10]. Consequently, it has motivated the development of new synthesis procedures to produce cathode materials with ultrafine and uniform nanoparticle size distribution.

Flame spray pyrolysis (FSP) has huge potentials in synthesizing ultrafine and pure nanoparticles [12–15]. Generally, FSP starts with aerosol precursor solutions, from which small precursor droplets are generated and then introduced to a high-temperature reactor. These precursor droplets undergo evaporation, coalescence, oxidation/decomposition, coagulation and sintering processes [16], involving interactions across liquid, gas and solid phases. The FSP synthetic method possesses several advantages, including low cost, high flexibility and easy scalability. Additionally, the solution-based FSP approach provides homogenous precursor mixtures and facilitates the production of small-sized nanoparticles with uniform distribution, compared with the traditional solid-state reaction method [17]. To yield better atomization quality of the precursor, experimental apparatuses, such as an ultrasonic nebulizer incorporating an inertial impactor [9,18], have been

^{*} Corresponding author.

E-mail address: k.luo@ucl.ac.uk (K.H. Luo).

<https://doi.org/10.1016/j.energy.2025.138010>

Received 22 March 2025; Received in revised form 16 July 2025; Accepted 11 August 2025

Available online 15 August 2025

0360-5442/© 2025 The Authors. Published by Elsevier Ltd. This is an open access article under the CC BY license (<http://creativecommons.org/licenses/by/4.0/>).

employed to generate ultra-fine precursor droplets with a narrow size distribution prior to FSP. The droplets within the precursor spray can be on the order of tens of nanometers in diameter [19], as determined by high-speed camera and other analytical methods. For instance, isolated droplets along the flame spray of lithium cobalt oxide were characterized to be around 50 nm in diameter [19], and these droplets were anticipated to disintegrate into even smaller droplets upon entering the flame, prior to nanoparticles synthesis.

Exploring the intrinsic mechanisms of nanoparticles formation from aqueous precursor mixtures is the prerequisite for further improvement and design of advanced nanomaterials via FSP. Many efforts have been devoted to clarifying the dominant factors in nanoparticles formation using FSP [14–16,18–21]. Meierhofer et al. demonstrated the influence of combinations of lithium and titanium precursors and solvents on nanoparticles formation [14]. They comprehensively evaluated the morphology and electrochemical performance, including the rate capability and charge reversibility for the synthesized nanomaterials. Angel et al. aimed to elucidate the combined effect of initial size and velocity of injected precursor droplets [20], through employing a dispersion gas flow during FSP for the production of perovskite nanomaterials. They proposed that increasing dispersion gas flow promotes the transition from droplet-to-particle to gas-to-particle formation mechanism, which can be explained by the decreased size of precursor droplets, leading to the modifications in the occurrence of droplet's explosion, flame temperature and particle residence time. Despite such findings, a thorough understanding of nanoparticles formation remains a subject due to high uncertainties in practical FSP, involving high complexity associated with air entrainment, flame radiation and instability induced by spray injection [22].

To gain fundamental insights into the mechanism of nanoparticles formation, studies with simplified configurations containing only a single isolated precursor droplet are necessary, particularly involving the initial size effect for precursor droplets. Primarily, considering volatility difference and gas decomposition in precursor mixtures, explosion is likely to occur for the precursor droplets exposed at FSP-like conditions [14–16,20,21]. The explosion behaviour can promote the production of fine-sized homogeneous nanoparticles, whilst excessively high explosion intensity may cause flame extinction and formation of large-sized inhomogeneous nanoparticles [14,20,21]. Notably, the droplet explosion process highly depends on the initial droplet size [14–16,23], and the variations in onset and intensity of droplet's explosion caused by the size effect can in turn affect the quality of synthesized nanoparticles. Several researches have explored the impact of explosion in micrometer-sized droplets composed of highly reactive FSP precursors, using experimental characterizations [14–16] or continuum-based one-dimensional simulation studies [23]. Generally, these micrometer-sized droplets initially exhibited quasi-steady combustion behaviour following the classical diffusion-controlled combustion droplet diameter squared (D^2) law, before experiencing shell formation and explosion processes. Whether or not the nanometer-sized precursor droplets retain similar morphological characteristics as micrometer-sized droplets remains unclear. Additionally, based on several continuum-based models, the superheating degree and probability of droplet explosion can be evaluated using the Lewis number to describe the competitions of diffusive mass transport and heat conduction [23]. However, the reliability of this continuum-based model becomes questionable for small droplets (below a micrometer in diameter) under FSP-like conditions with extremely high variation rates of temperature and species. This is due to neglected factors such as the droplet curvature and pressure difference between the droplet and its surroundings, making it unsuitable for providing an in-depth understanding of nanoparticles formation mechanism.

In general, for nanometer-sized metal precursor droplets, little is known about the role of initial size in the droplet's reaction kinetics accompanied by explosion, and subsequent nanoparticles growth under spray flame pyrolysis-like conditions [24]. The aim of this study is to

shed light on the initial size effect of lithium nitrate precursor droplets on the evaporation, oxidation and decomposition processes of droplets, and formation of lithium nanoparticles. A series of reactive force-field (ReaxFF) molecular dynamic (MD) simulations [25] will be carried out, with each simulation involving a single precursor droplet under high-temperature oxygen-containing condition. The size effect will be clarified through comprehensive analyses of droplet's morphology and potential and kinetic energy evolutions, bond kinetics, atomic motion, gas decomposition as well as the synthesized lithium-containing nanoparticles.

2. Results and discussion

2.1. Size effect of precursor droplet on reaction kinetics and nanoparticles formation

In this section, fundamental atomistic insights into the influence of the initial size of precursor droplets on the evaporation, oxidation and decomposition processes, and the subsequent nanoparticles formation in the oxygen-containing ambient at 3000 K and 1 MPa, will be unraveled through ReaxFF MD simulations. In this study, the droplet refers to the nano-sized precursor droplet. The pyrolysis and subsequent reaction of the droplet lead to the formation of small nanoparticles and, possibly, clusters of several nanoparticles. Several studies have suggested a high probability of explosion for the metal nitrate precursor droplets, as discussed above. To visualize intrinsic structural variations within the droplets, Fig. 1 presents the droplet slices in the $y \times z$ direction at different time instants, with a slice thickness of 3 nm. Fig. 2a–f present the temporal evolutions of droplet's diameter, normalized volume, interfacial density, normalized total atom number, and normalized variations in the total energy and potential energy for the droplets, respectively. Herein, the normalized droplet volume is calculated as the ratio of the droplet volume to its value at the start of the simulation. Similarly, the normalized total atom number as well as the normalized variations in total energy and potential energy for droplets are determined, which reflect the relative variations in morphology, mass transfer and energy for droplets with various initial sizes. Fig. 3 exhibits the radial distribution profile of density at several time instants, for the case of a droplet with an initial diameter of 8 nm.

Under the specific high-temperature condition, the droplet keeps expanding throughout its entire lifetime, as observed from the droplet snapshots in Fig. 1 and profiles of droplet size in Fig. 2a and b. Taking the droplet with an initial diameter of 8 nm as an example, its diameter and normalized volume increase continuously to 27.8 nm and 40.4, respectively, by the end of the droplet lifetime (8 ps). The steadily expanding droplet size is related to the formation of hollow structure within the droplet during the evaporation, oxidation/decomposition process, as evidenced from the droplet snapshots in Fig. 1a. This can be confirmed by the gradually decreasing density at the droplet core and the relatively higher interfacial density, as displayed in Figs. 2c and 3. Besides, the total number of atoms within the droplet is decreased over time, whereas the droplet volume is increased, as seen in Fig. 2b and d, which also suggests a formation of sparse internal structure for the droplets. The underlying cause for the droplet's size/volume expansion should be explained by the competitions of gas accumulation within the droplet produced from thermal decomposition of lithium nitrate (tend to increase the droplet volume), and atom diffusion towards the surrounding through evaporation or bond breaking chemical reaction (causing a reduction in the droplet volume). The continuously enlarged droplet size indicates that the morphological characteristics of the studied nanometer-sized precursor droplets are dominated by gas decomposition under this specific condition.

To identify the gas released from precursor decomposition and its impact, the temporal evolutions of decomposed gaseous products and ratio of decomposed gaseous molecules to the total number of molecules inside the droplet are elucidated via the results in Fig. 4a and b,

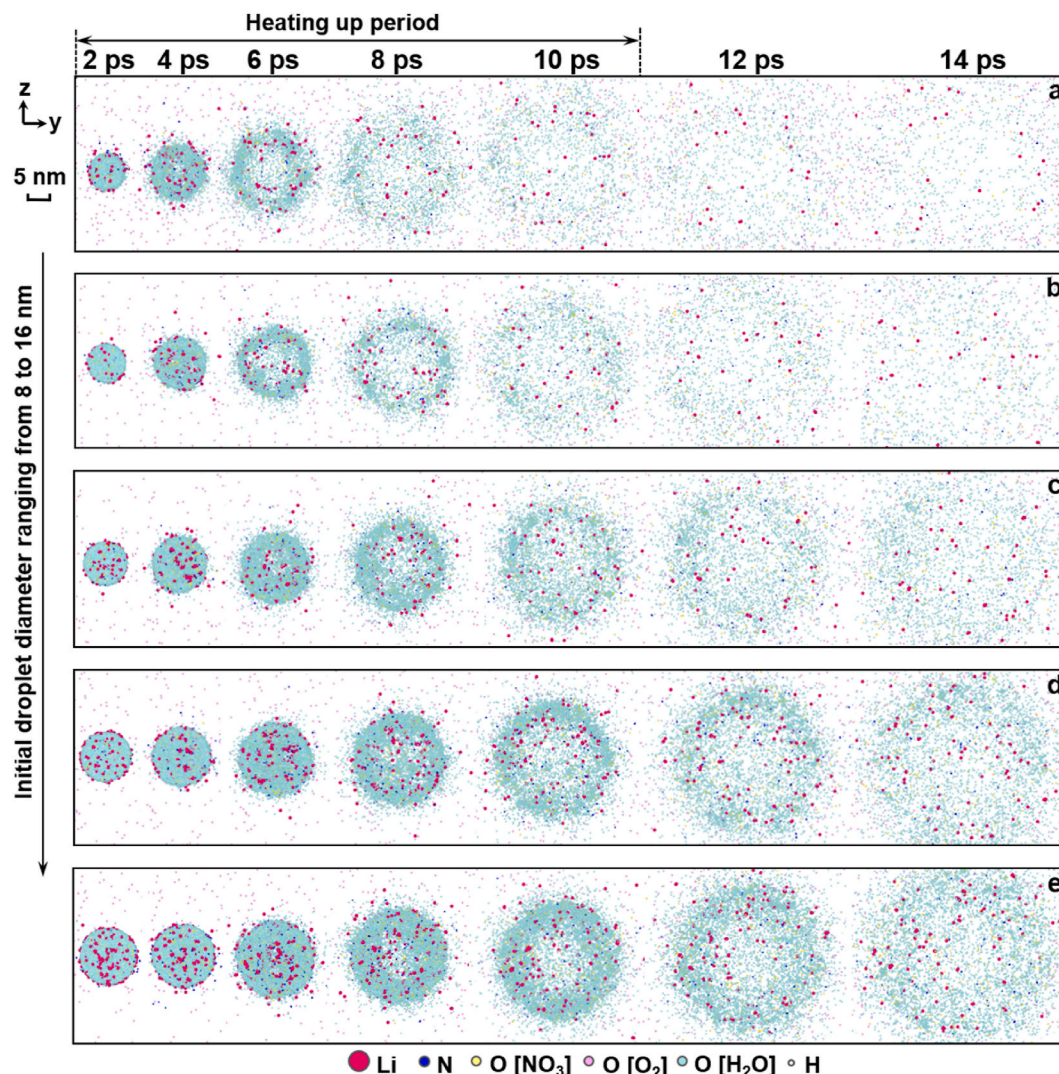


Fig. 1. Snapshots of lithium precursor droplets with an initial diameter of a) 8 nm, b) 10 nm, c) 12 nm, d) 14 nm, and e) 16 nm at different time instants. The circles in different colours refer to different atom types, and the size of circles is proportional to the atomic mass. The thickness of the slices in the $y \times z$ direction is 3 nm.

respectively. Fig. 5 shows the total energy of each atom at different time instants in the $y \times z$ direction, with a slice thickness of 3 nm, consistent with the setting in Fig. 1. As observed from Fig. 4a, the gaseous products in our simulation system primarily consist of nitrogen oxides, nitrogen and oxygen released from nitrates decomposition, along with hydrogen gas evolved from water thermolysis, which are aligned with experimental observations for nitrate precursors [26,27] and water decomposition [28] at extremely high temperatures. Throughout the droplet's lifetime, with the imposed heating condition using the Nosé–Hoover thermostat, the total energy of the droplet still keeps declining over time, as seen in Figs. 2e and 5. Herein, the droplet's total energy is calculated as the sum of potential and kinetic energy for each atom within the droplet, and the negative value of total energy, as observed in Fig. 5, is ascribed to the negative value of potential energy for each atom (the stronger appealing interactions between atoms, the smaller negative value of potential energy for these atoms). The monotonously decreasing trend of the droplet's total energy observed in Fig. 2e should be explained by the predominant role of precursor consumption during the evaporation and decomposition/oxidation processes, and the lesser role of thermal absorption, which enhances the droplet's kinetic energy.

When the droplet's initial diameter is increased from 8 to 16 nm, the explosion phenomenon is captured for all droplets, as depicted from the snapshots in Fig. 1 as well as the variations in the droplet diameter and

normalized volume in Fig. 2a and b. As the initial size of the droplet increases, more gas molecules are released from the thermal decomposition of the nitrate precursor as expected, due to the greater amount of precursor introduced into the droplet with an identical concentration. However, for large-sized droplets, more energy is required to disrupt the droplet, as the large droplet typically possesses more energy to maintain its spherical shape (larger surface energy or tension from the macroscopic perspective) by the increased number of atoms at the surface, as reflected by the increased interfacial density in Fig. 2c. Whether or not the increased decomposed gas caused by the increased droplet size will influence the occurrence or intensity of the droplet explosion remains to be revealed.

Based on our observations using MD, though more decomposed gas is released and trapped inside the droplet, as displayed in Fig. 4a, the explosion behaviour appears to be less intense, as the initial droplet size increases. This can be inferred from the decreased normalized droplet volume in Fig. 2b, or from the comparable droplet's diameter after 8 ps for the droplets with initial diameter ranging from 12 to 16 nm in Fig. 2a. The less vigorous explosion phenomena for large-sized droplets should be explained by the insufficient amount of decomposed gaseous molecules to trigger an explosion of the same intensity, using the same precursor concentration. At the initial stage of the heating up period (before 2 ps), the ratio of decomposed gas relative to the total atom

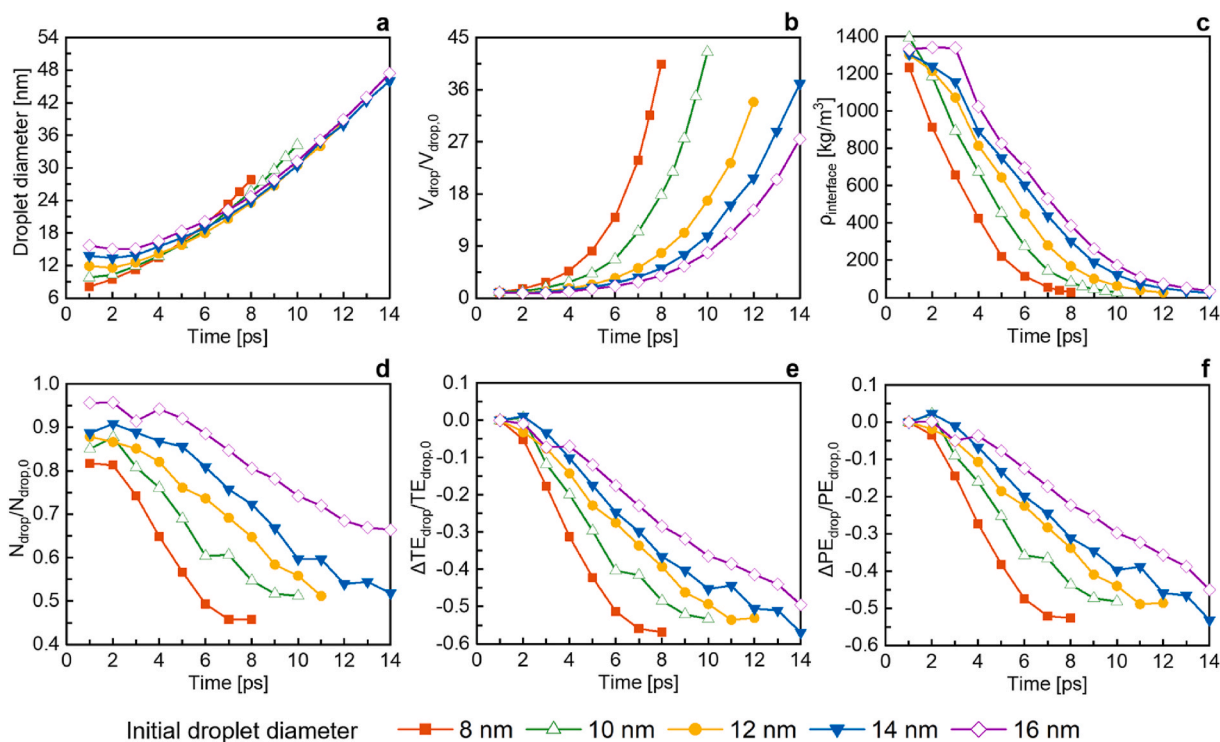


Fig. 2. Impact of initial droplet size on droplet dynamics, indicated by temporal evolutions of a) droplet diameter, b) normalized droplet volume, c) interfacial density, d) normalized atom number within the droplet, e) normalized variation of the droplet's total energy, and f) normalized variation of the droplet's potential energy. The equivalent droplet volume is calculated based on the defined equivalent droplet diameter.

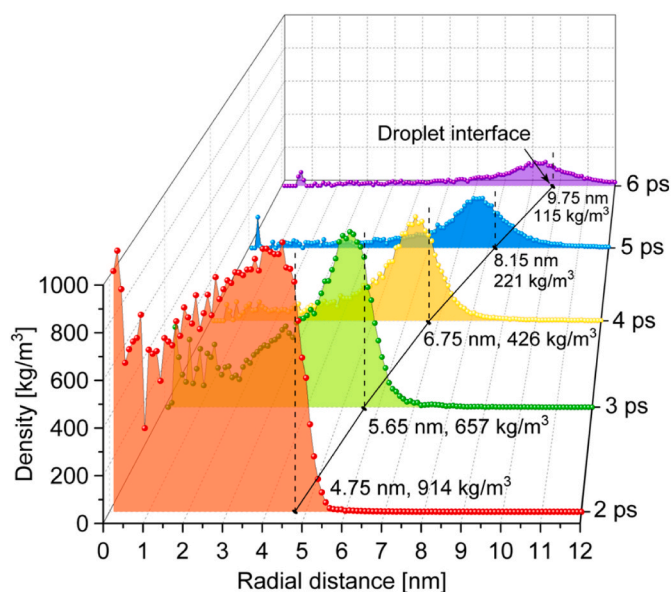


Fig. 3. Radial distribution profile of density at several time instants for the case of a droplet with an initial diameter of 8 nm. The origin of this figure corresponds to the centre of the precursor droplet. The droplet interface location and its density at different time instants are listed in this figure.

number inside the droplet is comparable among different droplets, as depicted in Fig. 4b. As the thermal decomposition of the lithium nitrate precursor proceeds, with the droplet diameter increasing from 8 to 16 nm, the atomic fraction of decomposed gas is apparently decreased from 0.0022 to 0.0011 at 4 ps (the difference of 0.0011). At the later stage of the heating up period (8 ps), the difference further increases to 0.0018. The explosion with identical intensity for larger droplets can be expected

by increasing the concentration of precursor or additive into the droplet, as demonstrated in our previous study for droplets composed of precursor and urea additive in the Appendix A [29]. Meanwhile, from the energy perspective, the droplet's normalized total energy exhibits similar decreasing trends over time among different droplets, but with a slower decline rate as the droplet size increases, as described in Fig. 2e. The slower variation in the droplet's normalized total energy also suggests the less intense explosion or gas decomposition. More concretely, the variation in the droplet's normalized total energy is primarily related to the droplet's normalized potential energy, as presented in Fig. 2e and f. The slower variation in droplet's normalized potential energy intrinsically reflects the relatively gradual weakened interaction potentials, caused by the transition from the liquid-state precursor to decomposed gas products. Based on the above observations, it can be concluded that under the specific high-temperature condition, the droplet's initial size has a crucial role in the droplet's morphology and explosion, mainly through varying the quantity of accumulated gas within the droplet from precursor pyrolysis.

Besides the droplet's explosive behaviours, the formation of lithium clusters becomes more pronounced when the initial droplet size increases, as evidenced by the larger lithium nanoparticles shown in pink in Fig. 1. To quantify the size effect on the lithium clusters formation, atomic motion and bond connections, Fig. 6a–h present the temporal evolutions of normalized proportions of lithium nanoparticles containing specific number of lithium atoms, mean squared displacements (MSDs) for all atoms and lithium atoms, as well as the normalized number for Li–Li, Li–N and Li–O bonds, respectively. When the initial droplet size is elevated from 8 to 16 nm, the normalized proportion of clusters containing only a single lithium atom is decreased from 0.83 to 0.61 by the end of the heating up period (10 ps), as depicted in Fig. 6a. Meanwhile, the normalized proportion of clusters with three lithium atoms and those with more than three lithium atoms ($m \cdot N_{\text{Li}m\text{O}x}/N_{\text{Li}}$, $m > 3$) are significantly increased from 0.029 to 0.094 and from nearly zero to 0.098, respectively, as compared in Fig. 6a and c.

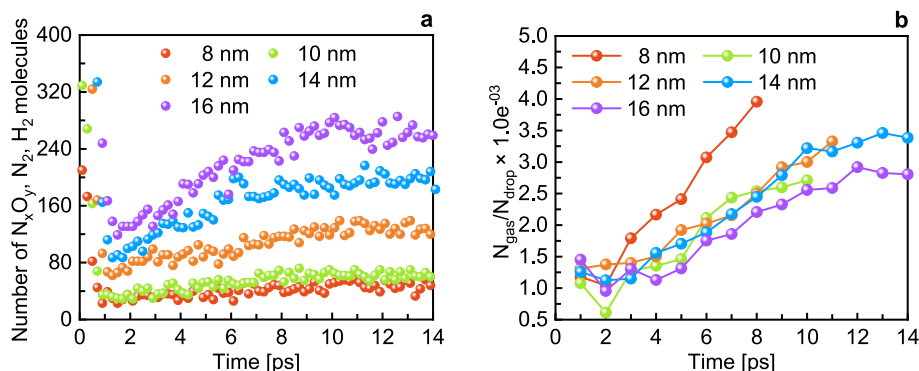


Fig. 4. Impact of initial droplet size on gas decomposition, indicated by temporal evolutions of a) molecular number of primary decomposed gas, b) ratio of decomposed gaseous molecules to the total number of molecules inside the droplet. The decomposed gas mainly consists of N_xO_y , N_2 and H_2 molecules.

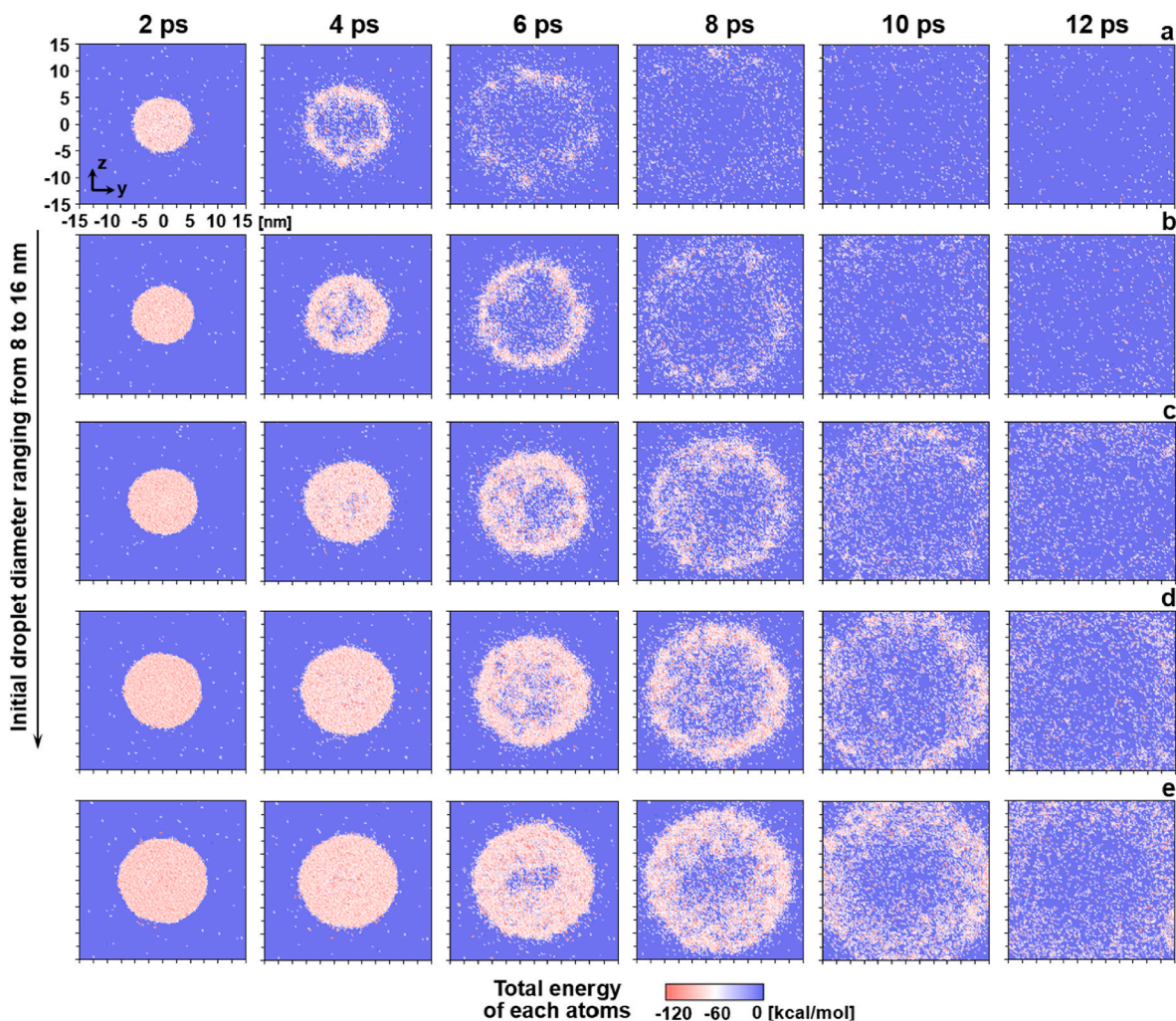


Fig. 5. Cross-sectional view of total energy in the case of a lithium precursor droplet with an initial diameter of a) 8 nm, b) 10 nm, c) 12 nm, d) 14 nm, and e) 16 nm at various time instants. The thickness of the slices in the $y \times z$ direction is 3 nm.

Correspondingly, the Li/O ratio of lithium oxides nanoparticles is increased from 0.70 to 0.86 at 10 ps. This suggests that more lithium atoms tend to agglomerate to form lithium nanoparticles, as the initial size of the precursor droplet becomes larger. Additionally, the decreased MSDs for all atoms and lithium atoms with the increased initial droplet size, as shown in Fig. 6d and e, also indicate the slower atomic motion and higher probability for the agglomeration of lithium nanoparticles.

Moreover, as the initial droplet size increases from 8 to 16 nm, the

proportion of Li-Li bonds relative to the total lithium atom number in the system (N_{Li-Li}/N_{Li}) also enhances, with its peak value rising sharply from 0.9 to 1.84, while the occurrence of this peak is slightly delayed, as observed in Fig. 6f. Similarly, for Li-N and Li-O bonds, their proportions increase from 0.82 to 1.01 and from 4.91 to 5.54, respectively, as seen in Fig. 6g and h. As the evaporation and oxidation/decomposition of the lithium precursor proceed, the clustering of lithium atoms seems to become less pronounced over time. By the end of the heating up period

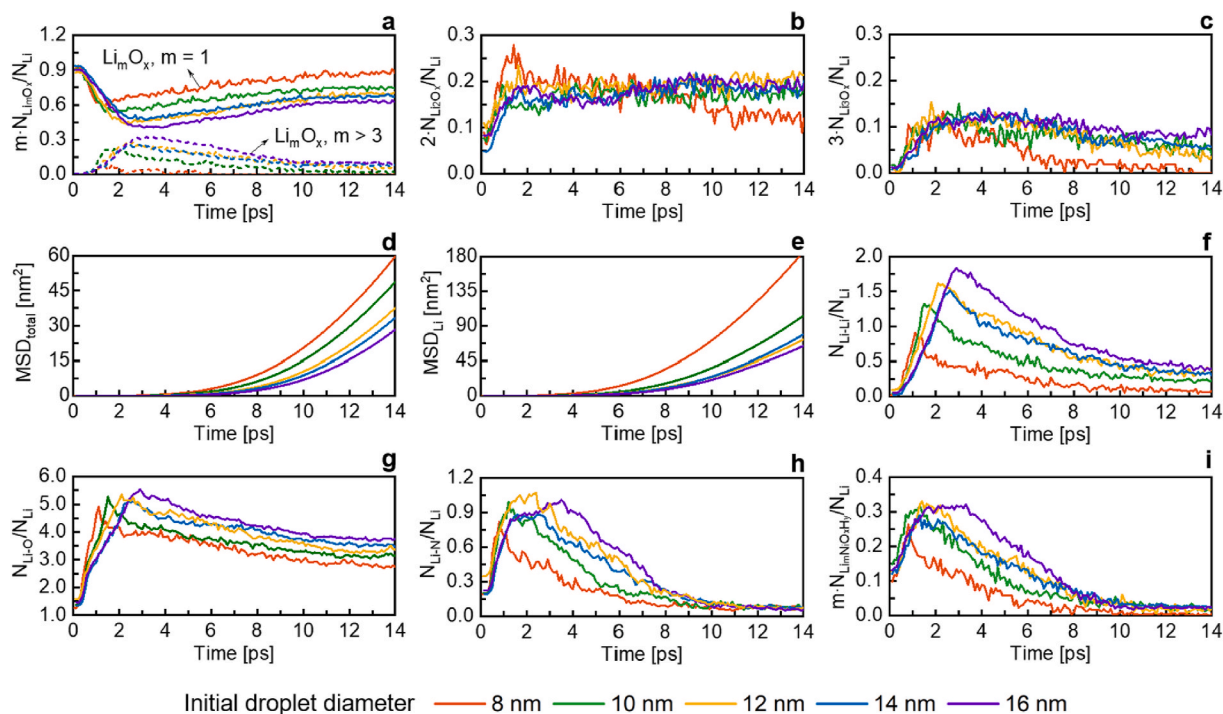


Fig. 6. Initial size effect of precursor droplet on lithium nanoparticles, atomic motion and bond connections. Temporal evolutions of normalized proportions of lithium nanoparticles containing a) a single lithium atom and more than three lithium atoms, b) two lithium atoms, and c) three lithium atoms. Temporal evolutions of mean squared displacement d) for all atoms and e) for Li atoms. Temporal evolutions of normalized number of f) Li–Li bonds, g) Li–N bonds, and h) Li–O bonds, and i) temporal evolution of normalized proportion of $\text{Li}_m\text{Ni}_x\text{O}_y\text{H}_z$ compounds.

(10 ps), the number of lithium bonds reaches almost equilibrated values. In particular, for Li–Li and Li–N bonds, the differences in the proportion of lithium bonds decrease from 0.94 to 0.4 and from 0.19 to 0.011, respectively. This is because the atomic motion is accelerated as the droplet's temperature rises (or with enhanced droplet's kinetic energy), leading to higher probability of cluster disruption or a lower proportion of lithium nanoparticles.

Specifically for the synthesized products with chemical formula of $\text{Li}_m\text{O}_x\text{Ni}_y\text{H}_z$, it contains all elements, i.e., lithium, nitrogen, oxygen and hydrogen atoms, in our studied simulation system. When the initial droplet diameter increases from 8 to 16 nm, the normalized proportion of this compounds relative to the total lithium number ($m \cdot N_{\text{Li}_m\text{O}_x\text{Ni}_y\text{H}_z} / N_{\text{Li}}$) is increased from 0.15 to 0.31 at the start of the heating up period (2 ps), as seen in Fig. 6f. By the middle of the heating up period (5 ps), it rises from 0.057 to 0.23, reflecting a greater disparity caused by the size effect at this moment. Nevertheless, by the end of the heating up period (10 ps), this difference becomes comparable across all simulation cases with droplets of varying initial sizes. This implies that while the initial droplet size plays a vital role in the formation of lithium nanoparticles at the early stage, its influence diminishes once the precursor droplet absorbs sufficient energy from the high-temperature environment to produce fine-sized nanoparticles.

To better understand the formation dynamics of $\text{Li}_m\text{O}_x\text{Ni}_y\text{H}_z$ clusters, Fig. 7 presents the reaction pathways of $\text{Li}_m\text{O}_x\text{Ni}_y\text{H}_z$ clusters in droplets with varying initial diameters. For the case with an initial droplet size of 8 nm, the lithium atoms are dispersed randomly in the precursor at 0.8 ps, as demonstrated in Fig. 7a. Subsequently, these atoms undergo agglomeration and aggregation, leading to the formation of $\text{Li}_6\text{O}_{16}\text{NH}_8$ and $\text{Li}_6\text{O}_6\text{NH}_3$ clusters at 0.9 ps. At 1.0 ps, these two clusters further combine to form $\text{Li}_7\text{O}_{28}\text{NH}_{28}$. When the initial droplet size increases to 10 nm, as shown in Fig. 7b, several small clusters containing single, two and three lithium atoms at 1.2 ps aggregate to form larger clusters comprising 10 and 13 lithium atoms at 1.3, 1.6 and 2.1 ps, respectively. With a further increase in droplet size from 10 to 16 nm, the size of the

formed clusters expands, containing 11, 17 and 18 lithium atoms, as seen in Fig. 7c–e. This phenomenon can be attributed to the inclusion of a greater number of lithium atoms within the simulation system, with the increased initial droplet size.

2.2. Size effect under lower ambient temperature condition

In practical FSP, the temperature varies significantly from location to location. In the periphery of the spray flame or at the downstream locations, the local temperature decreases due to air entrainment and mixing. In this section, the temperature effect is studied by decreasing the ambient temperature to 1500 K, while other conditions remain unchanged. To contrast the initial size effect of precursor droplets under the lower ambient temperature condition, Fig. 8 compares the proportions of nanoparticles containing different numbers of lithium atoms (Li_nX) at 10 ps, difference in normalized proportion of $\text{Li}_m\text{Ni}_x\text{O}_y\text{H}_z$, as well as the normalized Li–Li bond number at 10 ps ($N_{\text{Li-Li},10\text{ ps}}/N_{\text{Li}}$) and occurrence of the peak in the number of Li–Li bonds ($t_{p,\text{Li-Li}}$) at the ambient temperatures of 1500 and 3000 K.

When the ambient temperature decreases from 3000 to 1500 K, the probability of forming large-sized lithium clusters is markedly increased. Specifically for nanoparticles containing more than three lithium atoms (Li_{3+}X), as the initial droplet size increases from 8 to 16 nm, their proportion is increased from nearly zero to 10 % at 3000 K, whilst it is increased remarkably from 3 % to 33 % at 1500 K under the same condition, as shown in Fig. 8a and b. Conversely, the difference in the proportion of small-sized nanoparticles, such as LiX containing only a single lithium atom, is 22 % at 3000 K when the droplet size increases from 8 to 16 nm, while it is enlarged to 32 % at 1500 K. Specifically, for $\text{Li}_m\text{Ni}_x\text{O}_y\text{H}_z$ compounds, their proportion at two ambient temperatures is comparable for precursor droplets with small initial diameters, ranging from 8 to 12 nm, after the heating up period. Nevertheless, for the large-sized precursor droplets with initial diameters of 14 or 16 nm, the lower ambient temperature results in a dramatically higher probability of

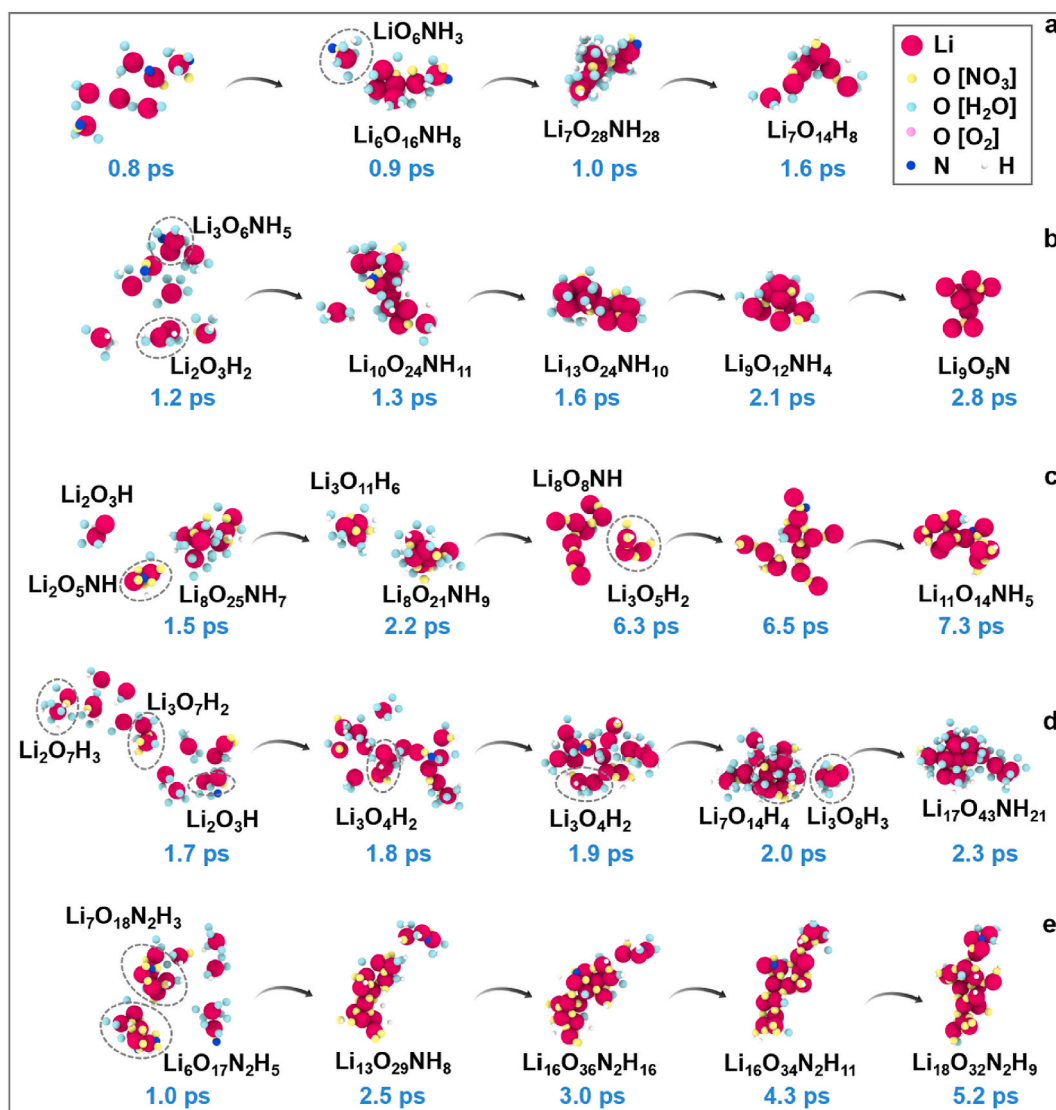


Fig. 7. Reaction pathways of lithium clusters in the case of a lithium precursor droplet with an initial diameter of a) 8 nm, b) 10 nm, c) 12 nm, d) 14 nm, and e) 16 nm at various time instants.

$\text{Li}_m\text{N}_i\text{O}_x\text{H}_y$ compounds, indicated by the positive value of $\Delta(m \cdot \text{N}_{\text{Li}}/\text{N}_{\text{Li}})/\text{N}_{\text{Li}}$ in Fig. 8c. These changes in the proportion of Li_nX and the size of generated lithium nanoparticles can be inferred from the variation in the lithium bond connections at the lower temperature. The difference in the normalized number of Li–Li bonds caused by the size effect of precursor droplets increases as the ambient temperature decreases, especially for large droplets with an initial diameter greater than 12 nm, as seen in Fig. 8d. Additionally, the occurrence of the peak in the number of Li–Li bonds is slightly delayed at the lower ambient temperature. These results indicate that the size effect of precursor droplets has a proportionally more pronounced effect on the size of synthesized lithium clusters at lower ambient temperature. This can be attributed to reduced reactivity of lithium atoms and increased stability of formed lithium clusters, due to decreased heat transfer from the ambient.

When the precursor droplet is exposed to the high-temperature environment for a sufficient duration (after 10 ps), the formation of lithium oxides is observed to be almost insensitive to the ambient temperature. For the lithium precursor droplet with an initial diameter of 8 nm, the decreasing ambient temperature from 3000 to 1500 K only leads to a slight decrease in the quasi-steady Li/O ratio from 0.64 to 0.60, as seen in Fig. A1 in the Appendix. In addition, the impact of the initial

droplet size also becomes relatively small, which can be explained by the dominance of gas-phase combustion kinetics after the precursor droplet fully evaporates.

3. Conclusions

In this study, the role of the initial size of lithium nitrate precursor droplets in the evaporation, oxidation and decomposition processes, and the subsequent nanoparticles formation, has been elucidated under the flame spray pyrolysis conditions. A series of reactive molecular dynamics simulations are performed for the precursor droplets with an initial diameter ranging from 8 to 16 nm, followed by extensive investigations into the droplet's morphology and energy evolution, bond connections, gas decomposition and formation kinetics of lithium nanoparticles. An explosive phenomenon is observed for all droplets, characterized by a continuously enlarging droplet volume, an internal hollow structure, and distinct interfacial density profiles. The monotonously expanding droplet volume should be ascribed to the predominant role of decomposed gas accumulation in shaping the droplet morphology, rather than the diffusion of molecules towards the environment following the evaporation and chemical reactions. As the initial size of precursor droplet increases, despite higher accumulation of

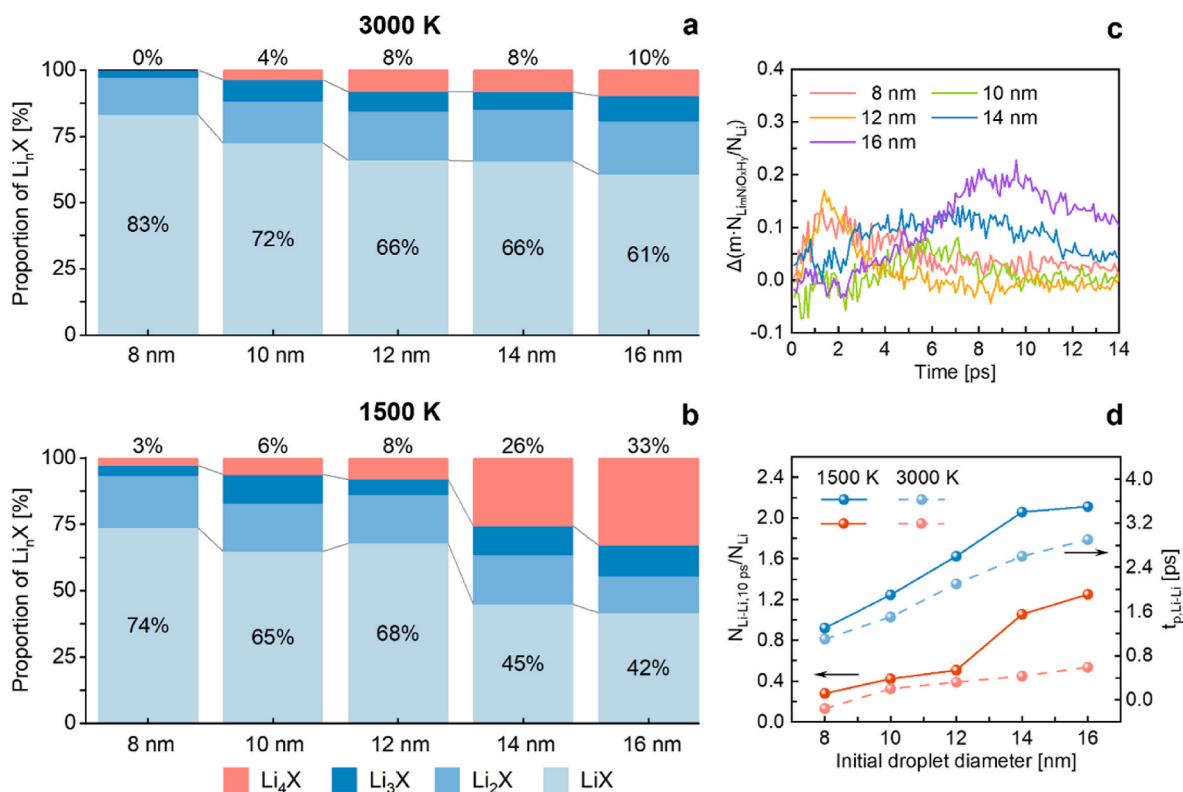


Fig. 8. Size effect of precursor droplet on formation of lithium nanoparticles at different ambient temperatures. a–b) Proportions of Li_nX containing different numbers of lithium atoms at 10 ps at 3000 and 1500 K, respectively, c) Temporal evolution of the difference in normalized proportion of $Li_mN_xO_yH_z$, d) Normalized number of Li–Li bonds at 10 ps and the occurrence of the peak in the number of Li–Li bonds.

decomposed gas trapped inside the droplet, the explosive behaviour of droplets becomes less intense, as inferred by the reduced normalized droplet volume. This can be explained by the reduced ratio of accumulated gaseous molecules to the total number of molecules within the droplet.

More significantly, the initial droplet size plays an essential role in the formation kinetics of lithium nanoparticles. More lithium atoms are prone to agglomerating to form lithium nanoparticles with greater size, as reflected by the increased normalized lithium bonds and slower atomic motion. The results of the reaction pathway also infer that randomly dispersed small lithium nanoparticles, which contain single, two and three lithium atoms, ultimately merge to form larger lithium clusters: the larger the initial droplet size, the larger the product lithium clusters. Furthermore, this size effect on the synthesis of fine-sized nanoparticles is observed to vary in relation to the ambient temperature. When the droplet is gradually heated up over time or exposed to a lower ambient temperature, the size effect becomes more pronounced on the size of formed lithium clusters, due to reduced reactivity of lithium atoms and increased stability of formed lithium nanoparticles. These findings highlight the intricate relationship among the initial precursor droplet size, reaction kinetics and quality of formed lithium nanoparticles via the flame spray pyrolysis, which will inspire further improvement in techniques for synthesis of nanomaterials. Specifically, a higher combustion temperature and a smaller initial size of the precursor droplets tend to promote the formation of smaller lithium oxide nanoparticles.

4. Simulation methodology and setup

In this study, a series of ReaxFF MD simulations [25] of lithium nitrate precursor droplets exposed to flame spray pyrolysis condition is performed using the LAMMPS package. Unlike the classical MD simulation method, the ReaxFF method can predict bond formation and

breaking due to the adopted bond order-based concept, which calculates the bond distance from the contributions of σ , π , and $\pi\pi$ bonds [30]. Besides valence interactions, the non-bonded interactions, including Coulombic and van der Waals forces, are calculated between each pair of atoms. The ReaxFF model optimizing for Li, N, O and H elements is utilized in this study [31], which was trained based on a dataset containing bond dissociation curves and equations of state by quantum mechanics calculations. This force field has been extensively validated against experimental data, such as the heat of formation for various Li crystalline phases [31].

In each simulation case, a single precursor droplet is placed at the center of a cubic simulation box, with each side measuring 100 nm. The droplet with an initial diameter ranging from 8 to 16 nm, is comprised of lithium nitrate dissolved in water, with a solution concentration of 1 mol/L H_2O . It should be noted that the studied nitrate is one of the most commonly used precursors in FSP, due to its low cost and high solubility in polar organic solvents [32]. The lithium nitrate and water molecules are randomly distributed within the droplet prior to each simulation. The region outside the droplet is occupied by oxygen molecules to simulate the oxygen-containing spray flame pyrolysis-like environment. The ambient pressure and temperature are set as 1 MPa and 3000 K or 1500 K, respectively, and the simulation system involves a total of 0.1–0.4 million atoms, depending on the initial droplet size and ambient temperature. The relative velocity between the droplet and the ambient is not included. At the start of each simulation case, the droplet's temperature is set as 300 K, and reaches the ambient temperature in 10 ps utilizing the Nosé–Hoover thermostat [33], which is termed as the heating up period. Afterward, the droplet temperature is maintained as the same as the environment, using the commonly-used canonical ensemble (NVT), with constant particles number, volume and temperature throughout the simulation. It should be noted that if this forced heating method is not applied (bringing the droplet to reach the desired temperature in a specified duration), the thermal absorption rate of the

droplets is extremely low, which would be too costly for the whole simulations of droplet disruption using the ReaxFF MD method. The periodic boundary condition is applied in the x, y and z dimensions, and the simulation timestep is 0.1 fs. In this study, the interface between the droplet and surrounding is determined based on the '90-10' method [34, 35], and the corresponding droplet's diameter and volume along with the total atom number within the droplet can be derived. The occurrence of droplet explosion is defined as the moment when the droplet no longer maintains its integrity as a whole, which can be determined based on the snapshots of the droplet slice as well as the density profile at the droplet interface. To identify the bond connections among various atoms or compounds formation, the widely used bond-order cutoff criterion of 0.3 Å is applied [35,36].

CRedit authorship contribution statement

Ruitian He: Writing – original draft, Visualization, Validation, Software, Methodology, Investigation, Formal analysis, Conceptualization. **Jingqi Gao:** Data curation, Formal analysis, Investigation, Software, Writing – review & editing, Visualization. **Kai H. Luo:** Writing – review & editing, Supervision, Project administration, Funding acquisition, Formal analysis, Conceptualization.

Declaration of competing interest

The authors declare that they have no known competing financial interests or personal relationships that could have appeared to influence the work reported in this paper.

Acknowledgements

The work is supported by the UK Engineering and Physical Sciences Research Council (EPSRC) under Grant No. EP/T015233/1. ARCHER2 supercomputing resources provided by the EPSRC under the project "UK Consortium on Mesoscale Engineering Sciences (UKCOMES)" (Grant No. EP/X035875/1) are also acknowledged. This work made use of computational support by CoSeC, the Computational Science Centre for Research Communities, through UKCOMES.

Appendix A. Supplementary data

Supplementary data to this article can be found online at <https://doi.org/10.1016/j.energy.2025.138010>.

Data availability

No data was used for the research described in the article.

References

- [1] Yoshino A. The birth of the lithium-ion battery. *Angew Chem Int Ed* 2012.
- [2] Tran Huu H, Vu NH, Ha H, Moon J, Kim HY, Im WB. *Nat Commun* 2021;12(1):3081.
- [3] Barai P, Feng Z, Kondo H, Srinivasan V. *J Phys Chem B* 2019;123(15):3291–303.
- [4] Zang G, Zhang J, Xu S, Xing Y. *Energy* 2021;218:119504.
- [5] Jia J, Zhao L, Liu Z, Hao X, Huo L, Zhao Y, Yao Z. *Energy* 2022;242:122534.
- [6] Lee KT, Cho J. *Nano Today* 2011;6(1):28–41.
- [7] Wilberforce T, Abdelkareem MA, Elsaid K, Olabi AG, Sayed ET. *Energy* 2022;240:122478.
- [8] Abdelkareem MA, Qaisar A, Sayed ET, Shehata N, Parambath JBM, Alami AH, Olabi AG. *Energy* 2024;131127.
- [9] Nandiyanto ABD, Okuyama K. *Adv Powder Technol* 2011;22(1):1–19.
- [10] Purwanto A, Yudha CS, Ubaidillah U, Widiyandari H, Ogi T, Haerudin H. *Mater Res Express* 2018;5(12):122001.
- [11] Liu Z, Zhang J, Luo J, Guo Z, Jiang H, Li Z, Liu Y, Song Z, Liu R, Liu W, Hu W, Chen Y. *Nano-Micro Lett* 2024;16(1):1–11.
- [12] Teoh WY, Amal R, Mädler L. *Nanoscale* 2010;2(8):1324–47.
- [13] Laine RM, Marchal JC, Sun HP, Pan XQ. *Nat Mater* 2006;5(9):710–2.
- [14] Meierhofer F, Li H, Gockeln M, Kun R, Grieb T, Rosenauer A, Fritsching U, Kiefer J, Birkenstock J, Mädler L, Pokhrel S. *ACS Appl Mater Interfaces* 2017;9(43):37760–77.
- [15] Karaköse E, Çolak H. *Energy* 2024;2311346.
- [16] Li H, Rosebrock CD, Riefler N, Wriedt T, Mädler L. *Proc Combust Inst* 2017;36(1):1011–8.
- [17] Zhang SS, Allen JL, Xu K, Jow TR. *J Power Sources* 2005;147(1–2):234–40.
- [18] Wang WN, Purwanto A, Lenggono IW, Okuyama K, Chang H, Jang HD. *Ind Eng Chem Res* 2008;47(5):1650–9.
- [19] Jang H, Seong C, Suh Y, Kim H, Lee C. *Aerosol Sci Tech* 2004;38(10):1027–32.
- [20] Angel S, Schneider F, Apazeller S, Kaziur-Cegla W, Schmidt TC, Schulz C, Wiggers H. *Proc Combust Inst* 2021;38(1):1279–87.
- [21] Rosebrock CD, Wriedt T, Mädler L, Wegner K. *AIChE J* 2016;62(2):381–91.
- [22] Yang Z, Adeosun A, Kumfer BM, Axelbaum RL. *Fuel* 2017;199:420–9.
- [23] Kunstmann B, Wlokas I, Kohns M, Hasse H. *Appl Energy Combust Sci* 2023;15:100156.
- [24] Stodt MFB, Kiefer J, Fritsching U. *Appl Energy Combust Sci* 2023;15:100170.
- [25] Van Duin AC, Dasgupta S, Lorant F, Goddard WA. *J Phys Chem A* 2001;105(41):9396–409.
- [26] Yuvaraj S, Fan-Yuan L, Tsong-Huei C, Chuin-Tih Y. *J Phys Chem B* 2003;107(4):1044–7.
- [27] Hill SC, Smoot LD. *Prog Energy Combust Sci* 2000;26(4–6):417–58.
- [28] Ji M, Wang J. *Int J Hydrogen Energy* 2021;46(78):38612–35.
- [29] He R, Luo KH. *Chem Eng J* 2024;497:154822.
- [30] Mao Q, Feng M, Jiang XZ, Ren Y, Luo KH, van Duin AC. *Prog Energy Combust Sci* 2023;97:101084.
- [31] Yang MY, Zybin SV, Das T, Merinov BV, Goddard WA, Mok EK, Hah HJ, Han HE, Choi YC, Kim SH. *Adv Energy Mater* 2023;13(3):2202949.
- [32] Strobel R, Pratsinis SE. *Phys Chem Chem Phys* 2011;13(20):9246–52.
- [33] Evans DJ, Holian BL. *J Chem Phys* 1985;83(8):4069–74.
- [34] Lekner J, Henderson JR. *Mol Phys* 1977;34(2):333–59.
- [35] He R, Luo KH. *Nanoscale* 2024;16(34):16119–26.
- [36] Kowalik M, Ashraf C, Damirchi B, Akbarian D, Rajabpour S, van Duin ACT. *J Phys Chem B* 2019;123(25):5357–67.